Production of HCl in the OH + ClO Reaction: Laboratory Measurements and Statistical Rate Theory Calculations

Jennifer B. Lipson, Thomas W. Beiderhase, Luisa T. Molina, and Mario J. Molina*

Departments of Earth, Atmospheric, and Planetary Sciences and Chemistry, Massachusetts Institute of Technology, Cambridge, Massachusetts 02139

Matthias Olzmann

Institut für Physikalische Chemie, Universität Halle-Wittenberg, D-06099 Halle, Germany

Received: December 17, 1998; In Final Form: April 22, 1999

The branching ratio for the OH + ClO reaction has been measured using the turbulent flow technique with high-pressure chemical ionization mass spectrometry for the detection of reactants and products. In our earlier study, OD was used instead of OH due to the large HCl background produced by the ClO source (*J. Chem. Soc., Faraday Trans.* **1997**, *93*, 2665). Improvements to our experimental technique have significantly reduced this HCl background, thus making it possible to observe directly the production of very small concentrations of HCl ($\sim 10^9$ molecule cm^{-3}) from the minor channel of the OH + ClO reaction. At room temperature and $\sim$100 Torr pressure, the rate constant for this minor channel was determined to be $(9.5 \pm 1.6) \times 10^{-13}$ cm^3 $molecule^{-1}$ s^{-1} with a two standard deviation error limit, which remained unchanged when the pressure was increased to 200 Torr. The temperature dependence of the rate constant for this minor channel was also investigated between 207 and 298 K, and the data were fit to the following Arrhenius expression: $(3.2 \pm 0.8) \times 10^{-13} \exp[(325 \pm 60)/T]$ cm^3 $molecule^{-1}$ s^{-1}. The branching ratio for the HCl channel was determined to be 0.07 ± 0.03 at all pressures and temperatures investigated in this study. Statistical rate theory calculations were also performed on the OH + ClO reaction system and are in good agreement with the experimental results.

Introduction

One of the long-standing problems in modeling the chemistry of the upper stratosphere has been the inability of models to correctly predict ozone concentrations above ~35 km. Between 35 and 75 km, the lifetime of ozone is short relative to the time scale for transport, and so ozone is expected to be in photochemical equilibrium. However, models have consistently failed to reproduce the expected balance between production and loss of odd oxygen ($O + O_3$). Attempts to model ozone levels in the upper stratosphere and lower mesosphere have resulted in an overprediction of ozone loss rates by as much as 35% near 40 km.[2−13] This "ozone deficit" problem has been partially attributed to the failure of models to correctly reproduce the observed partitioning of chlorine in the upper atmosphere. The models tend to overestimate the amount of active chlorine (e.g., ClO) relative to the amount of stable chlorine (e.g., HCl) by as much as a factor of 2.[3−5,7,8,10−18] Since calculated O_3 levels are very sensitive to the partitioning of chlorine, an overprediction of active chlorine will lead to an underestimation of O_3, particularly near 40 km where the chlorine cycle has its maximum contribution to the odd oxygen loss rate.[12] Many studies have proposed that discrepancies between measured and calculated partitioning could be resolved by including an additional source of HCl in the models.

The reaction of OH with ClO has long been suggested as a possible source of HCl production in the upper stratosphere.[2−4,7−10,12,13,15−18] Although the major products of the OH + ClO reaction are HO_2 and Cl ($\Delta H°_{298K} = -1.3$ kcal mol^{-1}),

$$OH + ClO \rightarrow HO_2 + Cl \quad (1a)$$

the reaction also has a minor channel that produces HCl and O_2 ($\Delta H°_{298K} = -55.8$ kcal mol^{-1}):

$$OH + ClO \rightarrow HCl + O_2 \quad (1b)$$

Reaction 1b is thermodynamically feasible, but kinetically unfavorable because two bonds must be broken almost simultaneously. Ab initio and RRKM calculations have shown that the reaction most likely proceeds through an addition−elimination mechanism via a four-centered transition state.[19] The conversion of ClO to Cl in reaction 1a is a chain-propagating step in catalytic ozone depletion cycles because ClO and Cl are both active forms of chlorine. However, reaction 1b converts an active form of chlorine (ClO) into a more stable reservoir species (HCl). Since reaction 1b is a chain-terminating step, even a relatively small branching ratio leads to substantially less ozone depletion by chlorine-containing compounds.

Early attempts to measure the branching ratio of the OH + ClO reaction were unable to rule out an HCl yield of zero for the minor channel due to uncertainties in the data.[20−23] As a result, no consensus had been reached on the atmospheric significance of reaction 1b, and most atmospheric models did not include this channel in their reaction set. In 1997, our laboratory reported the first direct measurement of a product

* To whom correspondence should be sent.

10.1021/jp9847787 CCC: $18.00
Published on Web 08/04/1999

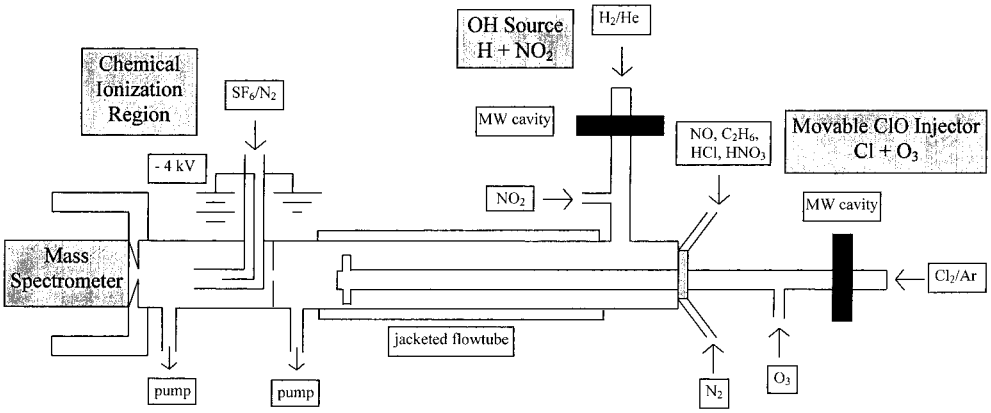

Figure 1. Schematic of experimental apparatus.

from reaction 1b.[1] In these branching ratio experiments, OD was used instead of OH due to the large HCl background produced by the ClO source. Since there was virtually no DCl background from the ClO source, we were able to observe production of very small concentrations of DCl ($\sim 10^9$ molecule cm^{-3}) over the experimental reaction time, which we positively identified as coming from the minor channel of the OD + ClO reaction. The branching ratio (k_{1b}/k_1) was determined to be 0.05 ± 0.02 at 298 K and 0.06 ± 0.02 at 210 K.

Several recent modeling studies of the upper stratosphere have shown that including a small branching ratio for the OH + ClO reaction has a dramatic effect on the partitioning of chlorine in their simulations. In fact, a very recent sensitivity analysis by Dubey et al.[19] found that reaction 1b is the most important source of uncertainty in modeled chlorine partitioning. In most of the modeling studies, including a branching ratio of ~6% essentially eliminated the discrepancies between measured and modeled chlorine partitioning for all altitudes and latitudes.[3,4,7,8,10,12,13,15−18] The addition of reaction 1b also helped to reduce the disagreement between measured and modeled ozone concentrations, especially near 40 km where the chlorine cycle has its maximum contribution to the odd oxygen loss rate.[2−4,7−9,12,13,18] However, above 45 km (where the HOx cycle is the dominant loss process), the models continue to overestimate ozone loss rates, possibly indicating a problem with calculated HOx partitioning.[6,9,12,13,24,25]

In our previous study of the branching ratio for the OD + ClO reaction, we clearly demonstrated that reaction 1b is a kinetically accessible product channel. Because of the demonstrated atmospheric importance of reaction 1b and because of the possibility of an isotope effect, it is essential to have branching ratio measurements for the OH + ClO reaction. Recent improvements to the experimental technique have significantly reduced the HCl background in our system, making it possible to detect the production of very small concentrations of HCl ($\sim 10^9$ molecule cm^{-3}) from channel 1b. In this article we describe our investigation of the branching ratio of reaction 1 conducted at pressures between 100 and 200 Torr and at a range of temperatures extending to those found in the lower stratosphere, using a turbulent flow tube coupled to a high-pressure chemical ionization mass spectrometer, a technique we developed in our laboratory.[26−28] We also present the results of statistical rate theory calculations on the OH + ClO reaction system. The comparison of experimental results with theoretical calculations is a good test of our understanding of the fundamental reaction dynamics of this system, as well as a test of our ability to predict kinetic isotope effects.

Experimental Section

A schematic of the experimental apparatus is presented in Figure 1. The setup is similar to that used in our previous study of OD + ClO.[1] However, several critical changes to the ClO production method have greatly reduced the HCl background in the system, as discussed in detail below. The flow tube (2.2 cm i.d., 120 cm long) was constructed of Pyrex tubing and coated with Halocarbon wax. A large flow of nitrogen carrier gas (40−75 STP L min^{-1}) was injected at the rear of the flow tube. The gases needed to generate OH were introduced through a sidearm (12 cm long, 6 mm diameter) located at the rear of the flow tube. ClO was generated in a double-nested movable injector, which consisted of an inner 6 mm alumina tube and an outer encasement made from corrugated Teflon tubing. The outer encasement was used so that the injector could be moved to various positions without breaking the vacuum seals, as well as to prevent ambient gases from condensing on cold portions of the injector. A Teflon device (described below) was placed at the end of the injector in order to enhance turbulent mixing. The electric discharge ion source was located between the temperature-regulated flow tube and the inlet to the quadrupole mass spectrometer. A variable-sized aperture (1.2−1.8 mm diameter) was used to create a pressure drop between the flow tube and the ion−molecule region. The size of the aperture was adjusted so that the pressure in the ion−molecule region remained roughly constant at 15 Torr, while the pressure in the flow tube was varied between 100 and 200 Torr. The pressures in the two regions were measured using MKS capacitance manometers (100 and 1000 Torr full scale). All gas flows were monitored with calibrated Tylan General mass flowmeters. For the low-temperature studies, Syltherm XLT (DOW Chemical Co.) was used as a coolant in the jacketed flow tube, and the nitrogen carrier gas was also precooled by passing it through a copper coil immersed in a liquid N_2 reservoir followed by resistive heating. The temperature, measured at both the entrance and exit points of the reaction region using copper−constantan thermocouples, was controlled to within 1 K.

The following gases were used as supplied or after further purification as described below: Ar (99.999%), He (99.999%), O_2 (99.994%), H_2 (99.999%), Cl_2 (>99.9%), NO_2 (99.5%), NO (>99.0%), C_2H_6 (>99.0%), and SF_6 (>99.99%).

As in our previous study, ClO was generated in the injector using the following reaction ($k_2 = 1.2 \times 10^{-11}$ cm^3 $molecule^{-1}$ s^{-1}):[29]

$$Cl + O_3 \rightarrow ClO + O_2 \qquad (2)$$

Chlorine atoms were produced by combining a ~5 STP L min^{-1}

flow of argon, which had passed through an inert gas purifier (Aeronex Gate Keeper, Model 500 K) with a ~1 STP mL min^{-1} flow of a 1% Cl_2/He mixture, which then passed through a microwave discharge produced by a Beenakker cavity operating at 70 W. To generate ClO, the chlorine atoms were mixed with a large excess of O_3 (~10^{13} molecule cm^{-3}) throughout the whole length of the movable alumina injector to ensure that only negligible amounts of chlorine atoms were introduced into the main flow. O_3, generated from an OREC ozonator and stored in a silica gel trap kept at ~−80 °C, was introduced into the system by passing a 3−20 STP mL min^{-1} flow of N_2 through the trap. Ozone partial pressures were determined by UV absorbance at 253.7 nm (Penray Hg lamp) in a 0.98 cm flow-through quartz cell.

There have been several important modifications to the ClO source since our previous study[1] that helped to reduce the HCl background in the system by more than 1 order of magnitude. In our previous study, the high level of HCl background (~10^{11} molecule cm^{-3}) in the system was observed to be coming primarily from the ClO source. This large background made it difficult to detect small amounts of HCl produced by channel 1b over the experimental reaction time. A significant portion of the HCl background was found to come from trace impurities of H_2 in the helium sweep gas used to flush Cl_2 through the microwave discharge. Although 99.999% pure helium was used, the manufacturer specifications indicate levels of H_2 up to 1 ppm. If 1 ppm of H_2 (~10^{12} molecule cm^{-3}) were present and sent through the microwave discharge in the presence of chlorine, it could certainly have produced enough H atoms to create a sizable HCl background. This HCl source was significantly reduced by installing an Aeronex inert gas purifier that removes H_2 impurities to sub-ppb levels. Another small source of HCl background came from the Cl_2—the UHP grade Cl_2 (>99.9% pure) used in this study contains small amounts of HCl impurities. We have changed the sweep gas through the chlorine microwave discharge from helium to argon. Argon increases the efficiency of Cl_2 microwave dissociation, making it possible to produce comparable amounts of ClO with lower initial Cl_2 concentrations, and thereby helped to reduce the HCl background in the system. Finally, another significant source of HCl background was identified as coming from the interaction of Cl atoms with the glass walls of the movable injector (particularly in the few centimeters after the chlorine microwave discharge, but before the introduction of excess O_3). This contribution to the HCl background was significantly reduced by switching to an injector made out of alumina. Overall, modifications to the ClO source have reduced the HCl background in the system by more than 1 order of magnitude (from ~5×10^{11} to <4×10^{10} molecule cm^{-3}), making it possible to observe production of very small amounts of HCl from reaction 1b. Decreasing the HCl background was critical to our ability to make accurate measurements of the branching ratio for the OH + ClO reaction. The background level was very stable during each experiment, but it varied somewhat from run to run as conditions, such as the initial ClO concentration, were changed.

In addition to the sources of HCl mentioned above, the production of HCl background by secondary reactions in the main flow tube was also a concern. For example, the products of the main channel of the OH + ClO reaction are HO_2 and Cl, which can react further to form HCl ($k_3 = 3.2 \times 10^{-11}$ cm^3 $molecule^{-1}$ s^{-1}):[29]

$$HO_2 + Cl \rightarrow HCl + O_2 \qquad (3)$$

Since reaction 3 is relatively fast, and HO_2 and Cl are the major products of reaction 1, reaction 3 was found to be the largest potential source of HCl background due to secondary chemistry. However, the large excess of O_3 (~10^{13} molecule cm^{-3}) used in the production of ClO also helped to scavenge Cl atoms produced by reaction 1a, and therefore, helped to minimize HCl background production from side reactions such as reaction 3.

As described in our previous study,[1] absolute ClO concentrations were determined by the titration reaction ($k_4 = 1.7 \times 10^{-11}$ cm^3 $molecule^{-1}$ s^{-1}):[29]

$$ClO + NO \rightarrow NO_2 + Cl \qquad (4)$$

and subsequent calibration of the NO_2 mass spectrometer signal. The NO was purified, using a method similar to that described in one of our earlier studies,[30] in order to reduce the background NO_2 contribution. An excess of ethane (~5×10^{13} molecule cm^{-3}), injected at the rear of the flow tube, scavenged the Cl atoms produced by the titration reaction in order to prevent regeneration of ClO due to the excess of O_3 used in the experiments. Modeling was used to correct for a slight underestimation of ClO concentration (≤15%) caused by the secondary reaction of C_2H_5 with NO_2. In our previous study of OD + ClO,[1] we demonstrated that our ClO titration technique yields linear calibration curves. For this study, ClO concentrations ranged from 5.0×10^{11} to 9.0×10^{11} molecule cm^{-3}.

For the branching ratio studies, OH was generated in the sidearm of the flow tube by the following reaction ($k_5 = 1.3 \times 10^{-10}$ cm^3 $molecule^{-1}$ s^{-1}):[29]

$$H + NO_2 \rightarrow OH + NO \qquad (5)$$

H atoms were generated by combining ~2 STP L min^{-1} flow of helium with ~0.5 STP mL min^{-1} flow of a 3% H_2/He mixture, which then passed through a molecular sieve trap immersed in liquid nitrogen and finally through a microwave discharge produced by a Beenakker cavity. The H atoms were then mixed with excess NO_2 to ensure that practically no hydrogen atoms were introduced into the main flow. The excess NO_2 helped to minimize production of background HCl from the following side reaction ($k_6 = 2.5 \times 10^{-11}$ cm^3 $molecule^{-1}$ s^{-1}):[31]

$$H + Cl_2 \rightarrow HCl + Cl \qquad (6)$$

Because OH was introduced through the sidearm, where the corresponding concentrations are ~30 times higher than in the main flow tube, the secondary reaction with NO_2 ($k_7 = 3.3 \times 10^{-12}$ cm^3 $molecule^{-1}$ s^{-1} at 100 Torr):[29]

$$OH + NO_2 + M \rightarrow HNO_3 + M \qquad (7)$$

was a concern in the production of OH by reaction 5. This difficulty was surmounted by using a relatively high flow of helium sweep gas through the H_2 microwave discharge in order to decrease the reaction time in the sidearm. Experimental conditions in the sidearm were optimized to ensure that reaction 5 went virtually to completion without significant loss of OH due to reaction 7. Although reaction 7 was minimized in the production of OH, this reaction provides a convenient titration method for determining absolute concentrations of OH, as demonstrated in our previous study of OH + ClO. A large excess of NO_2 was used to convert all of the OH into HNO_3 followed by calibration of the HNO_3 mass spectrometer signal using a bubbler containing 60 wt % HNO_3 solution maintained

at 0 °C. In our previous study,[1] we demonstrated that our OH titration technique yields linear calibration curves. OH concentrations used in this study ranged from 1×10^{11} to 4×10^{11} molecule cm^{-3}.

Absolute HCl concentrations were determined by calibrating the HCl mass spectrometer signal using a bubbler containing 20 wt % HCl/H_2O solution kept at 0 °C. For the low-temperature experiments, the HCl from the bubbler took a long time to equilibrate. For reasons of convenience, calibrations of the HCl signal at cold temperatures were also made by reacting an excess of H atoms with a known amount of Cl_2. The two methods of HCl calibration were in very good agreement.

Most of the chemical species relevant to this study (OH, ClO, HO_2, HCl, Cl_2, O_3, NO_2, and HNO_3) were chemically ionized with the SF_6^- reagent ion and then detected with the quadrupole mass spectrometer. SF_6^- was produced in the ion source by combining ~2 STP L min^{-1} flow of nitrogen with a 0.2 STP mL min^{-1} flow of a 5% SF_6/N_2 mixture, which then passed over the electric discharge. To confine the ionization process to SF_6 alone and to control the ion−molecule reaction time, another piece of Pyrex tubing (of variable length) was used to direct the SF_6^- downstream into the main flow tube effluent. More extensive descriptions of the ion source, ion lenses, and the quadrupole mass spectrometer are given in our earlier publications.[30,32]

In the chemical ionization scheme employed here, OH, ClO, Cl_2, O_3, and NO_2 are detected as their parent negative ions by charge-transfer reactions with SF_6^-. For example, OH is detected as OH^- through the following reaction:

$$SF_6^- + OH \rightarrow SF_6 + OH^- \quad (8)$$

HCl and HNO_3 are detected as $FHCl^-$ and $FHNO_3^-$ through fluoride-transfer reactions with SF_6^-:

$$SF_6^- + HCl \rightarrow SF_5 + FHCl^- \quad (9)$$

$$SF_6^- + HNO_3 \rightarrow SF_5 + FHNO_3^- \quad (10)$$

HO_2 is detected as $SF_4O_2^-$, generated presumably through a multistep pathway. The rate constants of many of the relevant ion−molecule reactions have been measured by Huey et al.[33] The ion−molecule region was kept at a lower pressure (15 Torr) than the flow tube (100−200 Torr). The drop in pressure lowered the concentrations of the neutrals in the ion−molecule region, thus decreasing the rates of potential ion−molecule side reactions. The lower neutral concentrations in the ion−molecule region also helped to prevent depletion of the SF_6^- reagent ions due to reaction with species in large excess such as O_3.

Results and Discussion

Branching Ratio Experiments. In our earlier work, we reported that our chemical ionization detection scheme resulted in sensitivities of 10^8-10^9 molecule cm^{-3} for NO_2, HO_2, and OH.[30] Although we did not carry out formal calibrations of the mass spectrometer for all the chlorine species detected with this method (Cl_2, ClO), it was apparent that these species could be detected with similar sensitivities. The mass spectrometer signals for these compounds were found to be linear over the range of concentrations used in this work. The stated sensitivity was more than adequate for the present work; in fact, it was necessary to degrade the sensitivity of the spectrometer (by decreasing the ion−molecule reaction time) to prevent the depletion of SF_6^- reagent ions due to reaction with species in large excess such as O_3.

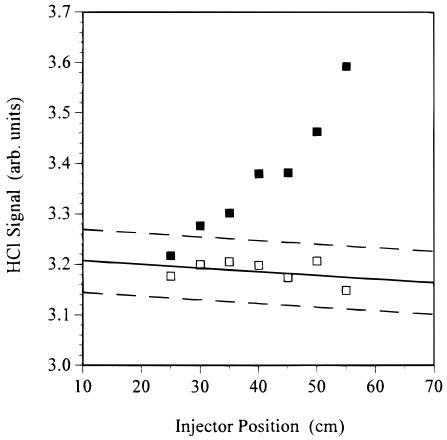

Figure 2. Observed production of HCl ([HCl] = 2.7×10^9 molecule cm^{-3}) from reaction 1b (black squares) above the small HCl background level (open squares) as a function of injector distance. A least-squares fit to the HCl background data was performed, and the dotted lines represent the $\pm 2\sigma$ level. This data set was obtained under the following conditions: $P = 97$ Torr, $T = 298$ K, average velocity = 1800 cm s^{-1}, Reynolds number = 3200, $[OH]_o = 1.8 \times 10^{11}$ molecule cm^{-3}, $[ClO]_o = 8.3 \times 10^{11}$ molecule cm^{-3}.

Because of the reduced HCl background in these experiments, we were able to observe production of very small concentrations of HCl (~10^9 molecule cm^{-3}) over the reaction time (~20 ms), which we have positively identified as coming from reaction 1b. Figure 2 shows that the rise of HCl is easily observed above the background noise. In Figure 2, the HCl rise (black squares) has been overlaid on the background signal (open squares) in order to demonstrate that the HCl rise is much larger than the $\pm 2\sigma$ level of the background noise. Under the optimal experimental conditions ([ClO] ~ 1×10^{12} molecule cm^{-3} and [OH] ~ 1×10^{11} molecule cm^{-3}), modeling shows that side reactions can only produce concentrations of HCl that are less than the detection limit of the instrument (~10^8 molecule cm^{-3}). Table 1 contains a list of the reactions used in the modeling. The following side reactions can produce HCl in our system:

$$HO_2 + Cl \rightarrow HCl + O_2 \quad (3)$$

$$H + Cl_2 \rightarrow HCl + Cl \quad (6)$$

$$Cl + H_2 \rightarrow HCl + H \quad (11)$$

In our experiments, the source conditions for OH and ClO are optimized in order to prevent stray H and Cl atoms from entering the main flow tube. Furthermore, reaction 11 is too slow to be important in our system ($k_{11} = 1.6 \times 10^{-14}$ cm^3 $molecule^{-1}$ s^{-1}).[31] Reaction 3 is more difficult to avoid because HO_2 and Cl are the products of reaction 1a, the main channel of the OH + ClO reaction. However, modeling shows that the large excess of O_3, used to generate ClO, is efficient in scavenging Cl atoms produced in the main flow tube. Under optimal experimental conditions, reaction 3 can only produce levels of HCl (~10^8 molecule cm^{-3}) that are below the detection limit of our instrument.

Computer modeling was used to extract a rate constant for reaction 1b by fitting the observed HCl production. The model input included the initial concentrations of ClO, OH, and all precursors. Table 2 contains a list of the initial conditions and calculated rate constants (k_{1b}) for the branching ratio experiments. The observed HCl signal was found to increase linearly

TABLE 1: Chemical Reactions Used in Computer Simulations for the Branching Ratio Studies

reaction	k^a (cm^3 $molecule^{-1}$ s^{-1})
$OH + ClO \rightarrow HO_2 + Cl$	1.46×10^{-11}
$OH + ClO \rightarrow HCl + O_2$	see text
$Cl + HO_2 \rightarrow HCl + O_2$	3.2×10^{-11}
$Cl + HO_2 \rightarrow OH + ClO$	9.1×10^{-12}
$Cl + O_3 \rightarrow ClO + O_2$	1.2×10^{-11}
$Cl + H_2 \rightarrow HCl + H$	1.6×10^{-14}
$Cl + NO_2 + M \rightarrow ClONO + M$	3.3×10^{-12}
$H + Cl_2 \rightarrow HCl + Cl$	2.5×10^{-11}
$H + O_3 \rightarrow OH + O_2$	2.9×10^{-11}
$H + NO_2 \rightarrow OH + NO$	1.3×10^{-10}
$OH + O_3 \rightarrow HO_2 + O_2$	6.8×10^{-14}
$OH + Cl_2 \rightarrow HOCl + Cl$	6.7×10^{-14}
$OH + OH \rightarrow H_2O + O$	1.9×10^{-12}
$OH + OH + M \rightarrow H_2O_2 + M$	1.4×10^{-12}
$OH + HO_2 \rightarrow H_2O + O_2$	1.1×10^{-10}
$OH + NO_2 + M \rightarrow HNO_3 + M$	3.3×10^{-12}
$OH + NO + M \rightarrow HONO + M$	1.7×10^{-12}
$OH + HCl \rightarrow H_2O + Cl$	8.0×10^{-13}
$ClO + ClO \rightarrow$ products	7.7×10^{-14}
$ClO + HO_2 \rightarrow HOCl + O_2$	5.0×10^{-12}
$ClO + NO \rightarrow NO_2 + Cl$	1.7×10^{-11}
$ClO + NO_2 + M \rightarrow ClONO_2 + M$	4.6×10^{-13}
$HO_2 + HO_2 \rightarrow H_2O_2 + O_2$	1.9×10^{-12}
$HO_2 + NO_2 + M \rightarrow HO_2NO_2 + M$	3.8×10^{-13}
$HO_2 + NO \rightarrow NO_2 + OH$	8.1×10^{-12}

[a] Rate constants are from refs 1, 29, and 31, at 298 K and 100 Torr.

over the experimental reaction time, as can be seen in Figure 2. Modeling confirms that the HCl signal is practically linear and does not approach its equilibrium level under typical experimental conditions and reaction times. The branching ratio for the OH + ClO reaction was measured at room temperature and at a pressure of 100 Torr under a variety of conditions to ensure that the results were independent of the initial concentrations. In experiment 5, close to optimal initial concentrations for OH and ClO were used, such that the observed HCl production was due to reaction 1b only. In experiment 1, the initial OH concentration was increased by 85% compared to experiment 5. Under these conditions, modeling shows that ~20% of the observed HCl production was due to the side reaction $HO_2 + Cl$. Despite the different initial conditions and the differing amounts of HCl production from side reactions, experiments 1 and 5 yielded the same rate constant for the minor channel ($k_{1b} = 10.2 \times 10^{-13}$ cm^3 $molecule^{-1}$ s^{-1}). Therefore, the modeling approach appears to correctly simulate the chemistry in our system, yielding branching ratio results that are independent of the initial conditions.

As expected, the fitting procedure used to calculate k_{1b} is sensitive to the initial concentrations of OH and ClO and to the observed concentration of HCl produced over a specific reaction time. These concentrations were measured to better than 30% accuracy; we found that these errors propagate linearly into the calculated branching ratio. The fitting procedure used to calculate k_{1b} is also affected by the other rate constants used in the model. For example, increasing the rate constant k_3 for the reaction $Cl + HO_2 \rightarrow HCl + O_2$ increases the proportion of HCl production coming from side reactions, and therefore decreases k_{1b}; however, a 50% increase in k_3 leads to only a 20% decrease in the calculated value of k_{1b}. Furthermore, the fitting procedure is not very sensitive to changes in the rate constant k_{1a} for the major channel of the OH + ClO reaction. For example, changing k_{1a} by 50% leads to less than 15% change in the calculated value of k_{1b}. In the modeling procedure we assumed that $k_{1a} = k_1$. This assumption was necessary in the initial analysis of the data when the value of k_{1b} was unknown. However, a reanalysis of one data set using $k_{1a} = k_1 - k_{1b}$ verified that our initial assumption introduced negligible error into the branching ratio measurements.

Although modeling shows that for optimal initial conditions the observed HCl production cannot be due to homogeneous side reactions, the possibility exists that the HCl could be a result of heterogeneous reactions on the wall of the flow tube. In our previous study of OD + ClO,[1] we performed two experiments to demonstrate that the observed DCl production was not due to heterogeneous processes. First, we checked that an uncoated tube gave results in very good agreement with those obtained with the Halocarbon wax-coated tube, indicating that the observed DCl production was not due to reactions on the wall of the flow tube. Second, the total pressure in the flow tube was increased by almost a factor of 2; the effects of heterogeneous processes are reduced at higher pressures,[26] and yet the branching ratio did not decrease, thus providing further evidence that the observed DCl production was not due to heterogeneous processes. In fact, the branching ratio for OD + ClO was observed to increase by ~35% at the higher pressure (180 vs 95 Torr). Considering experimental uncertainties, we were not able to draw any definite conclusions about the pressure dependence of the branching ratio. There are many examples of radical−radical reactions that proceed through an intermediate complex that is stabilized at higher pressures. However, in the case of OD + ClO, theoretical calculations indicate that the intermediate complex (DOOCl*) is not long-lived enough to be stabilized by collisions under atmospheric conditions.[19] This will also be discussed in detail below.

In this study, we have conducted a more thorough investigation of the pressure dependence of the OH + ClO branching ratio, and the results are presented in Table 2. The measured rate constants for the minor channel at 200 Torr are clearly within the range of the values for the 100 Torr experiments. In these experiments we did not see any evidence for a pressure effect on the rate constant of reaction 1b. Furthermore, in our previous work[1] we found the overall rate constant of the OH + ClO reaction (k_1) to be independent of pressure, as demonstrated by the good agreement between our measurements at 100 Torr and previous measurements at low pressure (~1 Torr).[22] We therefore conclude that the branching ratio of the OH + ClO reaction is independent of pressure for conditions relevant to the atmosphere. Two important modifications to the experimental apparatus have been made for these measurements, which might help to explain the slight discrepancy between the DCl and HCl experiments. The first modification was that the diameter of the aperture between the flow tube and ion−molecule region was varied in order to maintain a constant pressure in the ion−molecule region for the HCl measurements at 200 Torr. In the DCl experiments, the aperture size was kept constant even at higher pressures. Thus, the doubling of pressure in the flow tube from 95 to 180 Torr also created a doubling of pressure in the ion−molecule region. This doubling of neutral concentrations in the ion−molecule region may have contributed to an increase in secondary ion−molecule reactions that could have affected the DCl experiments at 180 Torr. The second modification to the experimental apparatus was that the shape of the turbulizer, on the end of the movable injector, was redesigned to better enhance turbulent mixing in the flow tube at increased pressures. In our DCl experiments, an open, fan-shaped turbulizer was used for the measurements at both 95 and 180 Torr. However, in recent mixing tests we found that a modified turbulizer design helped to improve mixing at 200

TABLE 2: Summary of Experimental Conditions and Results for the Branching Ratio Studies of the OH + ClO Reaction

expt no.	T (K)	P (Torr)	$[OH]_o$ (10^{11} molecule cm^{-3})	$[ClO]_o$ (10^{11} molecule cm^{-3})	k_{1b} (10^{-13} cm^3 molecule^{-1} s^{-1})	branching ratio (k_{1b}/k_1)
1	298	98	3.5	6.0	10.2	0.070
2	298	94	2.2	6.1	9.5	0.065
3	298	97	1.8	8.3	10.4	0.071
4	298	96	1.4	7.9	8.6	0.059
5	298	96	1.9	4.9	10.2	0.070
6	298	94	1.2	8.2	9.1	0.062
7	298	191	2.2	7.0	8.3	0.057
8	298	201	1.3	5.7	9.1	0.062
9	298	203	1.9	6.6	10.2	0.070
10	275	171	2.2	6.9	10.2	0.064
11	259	152	1.5	5.8	10.5	0.062
12	246	157	1.4	6.2	12.2	0.068
13	233	152	1.8	5.6	13.1	0.068
14	217	140	1.7	6.6	15.1	0.071
15	207	127	2.5	6.5	14.5	0.064

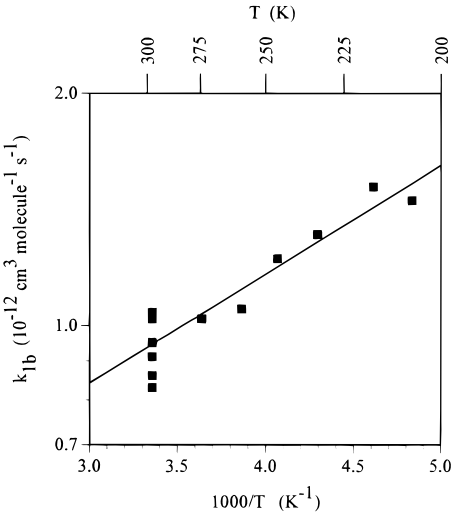

Figure 3. Arrhenius plot for the reaction OH + ClO → HCl + O_2. The least-squares fit to the data yields the expression $k(T) = (3.2 \pm 0.8) \times 10^{-13}$ exp[$(325 \pm 60)/T$] cm^3 molecule^{-1} s^{-1}.

Torr. In the new design, the gas in the movable injector is forced through a series of small holes punched in several pieces of Teflon tubing that protrude into the flow tube perpendicular to the direction of the main flow. All of the branching ratio studies for the OH + ClO reaction were conducted using this modified turbulizer design. In the DCl experiments at 180 Torr, insufficient mixing may have contributed to error in the measurement of the branching ratio. Overall, the discrepancy between the HCl and DCl measurements at higher pressures is certainly within the reported errors of the measurements. However, we believe that these two recent improvements to the apparatus have produced more accurate measurements of the branching ratio for the OH + ClO reaction at 200 Torr.

We performed several measurements of the branching ratio for OH + ClO at temperatures between 207 and 298 K in order to establish the temperature dependence of the rate constant k_{1b} for conditions relevant to the stratosphere. From the data listed in Table 2 and plotted in Figure 3, we obtain the Arrhenius expression $k_{1b}(T) = (3.2 \pm 0.8) \times 10^{-13}$ exp[$(325 \pm 60)/T$] cm^3 molecule^{-1} s^{-1}. The uncertainty represents the two standard deviation statistical error in the data and is not an estimate of systematic errors. The negative temperature dependence of k_{1b} indicates that reaction 1b goes through an intermediate complex.[34,35] The fundamental reaction dynamics of the OH + ClO system will be discussed in more detail in the next section describing the statistical rate theory calculations. The branching ratios (k_{1b}/k_1) reported in Table 2 were calculated using the measured Arrhenius expression for the overall rate constant of the OH + ClO reaction from our previous publication ($k_1(T) = (5.5 \pm 1.6) \times 10^{-12}$ exp[$(292 \pm 72)/T$] cm^3 molecule^{-1} s^{-1}).[1] The branching ratio for the OH + ClO reaction has been determined to be 0.07 ± 0.03; within the error of the measurement, the branching ratio does not appear to have a strong temperature dependence. The reported error for the branching ratio is an estimate of the systematic error and the uncertainty of the model fitting procedure based on a sensitivity analysis. In our previous studies of the OD + ClO reaction,[1] we found that the branching ratio to form DCl ranged from 0.05 ± 0.02 at 298 K to 0.06 ± 0.02 at 210 K. In the OH + ClO branching ratio studies at low temperatures, there may exist a slight trend toward increasing branching ratios at lower temperatures. However, within the error of the OH + ClO branching ratio measurements, it is difficult to identify a trend of <1%. Therefore, we conclude that the branching ratio is essentially independent of temperature under conditions relevant to the atmosphere. Overall, the isotope effect on the branching ratio appears to be small. The observed isotope effect and its agreement with theoretical predictions will be discussed further in the next section describing the statistical rate theory calculations.

TABLE 3: Comparison of Measured Branching Ratios for the OH + ClO Reaction

technique[a]	T (K)	P (Torr)	branching ratio (k_{1b}/k_1)	ref
DF-LF/RF	298	1.0−3.5	<0.35	20
DF-LF/RF	243−298	1.0−5.0	0.15 ± 0.2	21
DF-LF/LMR	293	1.0	0.14 ± 0.14	22
DF-LF/EIMS	298	0.5−0.9	0.02 ± 0.12	23
DF-TF/CIMS	211	100	0.06 ± 0.02	1
	298		0.05 ± 0.02	OD + ClO
DF-TF/CIMS	207−298	100−200	0.07 ± 0.03	this work OH + ClO

[a] Key: DF, discharge flow; LF, laminar flow; TF, turbulent flow; RF, resonance fluorescence detection; LMR, laser magnetic resonance detection; EIMS, electron impact mass spectrometry detection; CIMS, chemical ionization mass spectrometry detection.

Our results for the branching ratio of reaction 1 are consistent with the results of previous studies, which are listed in Table 3. Previous attempts to measure the branching ratio were unsuccessful in ruling out an HCl yield of zero for the minor channel, due to uncertainties in the results. Leu and Lin[20] and Burrows et al.[21] used chemical titration to convert the HO_2

formed by reaction 1a back into OH, which was then detected by resonance fluorescence. The ratio of [HO_2] formed (determined by the regeneration of OH) to [OH] lost was used to calculate the branching ratio. A problem with this indirect method is that the ratio of HO_2 formed to OH lost is not exactly equal to the branching ratio due to additional loss mechanisms for HO_2, such as self-reaction or reaction with other species in the system, i.e., Cl, OH, and ClO. Using this indirect method, Leu and Lin were able to place only an upper limit on the branching ratio. Burrows et al. modeled the system and found that a correction of almost 50% was necessary to convert the measured HO_2/OH ratio into a branching ratio. These authors measured the branching ratio between 243 and 298 K and found no temperature dependence, in agreement with our current results. Hills and Howard[22] were able to detect HO_2 directly using laser magnetic resonance. They measured the HO_2/OH ratio and then used modeling to extract the branching ratio, in a manner similar to Burrows et al. Of the four reported branching ratio studies, only Poulet et al.[23] were able to detect HCl using electron impact mass spectrometry. They measured the branching ratio by observing the HCl/OH ratio as the OH discharge was turned on and off at a fixed injector position. However, they did not have sufficient sensitivity to observe HCl production over the reaction time. As in the other studies, the errors were too large to rule out an HCl yield of zero. Because of the indirect methods used and the large reported errors, all four previous studies were unable to positively establish the existence of the minor channel. In contrast, our direct measurements of HCl production from reaction 1b over the experimental reaction time have positively established the existence and kinetic significance of the minor channel under atmospherically relevant conditions.

Modeling by Statistical Rate Theory. As already outlined above, the overall reaction is assumed to proceed via an addition−elimination mechanism.[19,21,36] To verify and rationalize the experimentally determined branching ratios and to characterize the influence of isotopic substitution, we performed a detailed modeling, using master equations and statistical rate theory. Moreover, the temperature and pressure dependence of the overall rate constant was examined, because an adequate description of these different quantities by a common model could provide additional evidence for the postulated mechanism.

Within this model, the reactions

$$OH + ClO \rightarrow HO_2 + Cl \tag{1a}$$

and

$$OH + ClO \rightarrow HCl + O_2 \tag{1b}$$

correspond to the following microscopic steps, where an asterisk denotes vibrational and rotational excitation:

$$OH + ClO \leftrightarrows HOOCl^* \tag{1}$$

$$HOOCl^* \leftrightarrows HO_2 + Cl \tag{1a′}$$

$$HOOCl^* \rightarrow HCl + O_2(a^1\Delta_g) \tag{1b′}$$

$$HOOCl^* + M \leftrightarrows HOOCl + M \tag{12}$$

Because the electronic ground state of the intermediate, HOOCl, is most likely a singlet state, reaction 1b′ is assumed to yield $O_2(^1\Delta)$ due to spin conservation.[19,21,36,37] The thermochemistry of the system is characterized by using the following heats of formation, $\Delta_f H°_{0K}$ (in kcal mol^{-1}): ClO, 24.4;[38] OH, 9.32;[38] Cl, 28.59;[38] HO_2, 4.18;[38,39] HOOCl, 1.5.[37]

The kinetic quantities of a chemical activation system can be derived by solving the appropriate master equation,[40−44] which describes the balance over all gain and loss processes for a given energy level, E_i, of the intermediate, i.e., in our case of HOOCl:

$$\frac{dn_i}{dt} = R_{form} f_i - \omega n_i + \omega \sum_j P_{ij} n_j - (k_{-1,i} + k_{1a',i} + k_{1b',i}) n_i \tag{13}$$

Here, $n_i = n(E_i)$ is the concentration of the intermediate with an internal energy E_i. R_{form} represents the overall rate of its formation and $f_i = f(E_i)$ its normalized nascent distribution function as generated by this formation reaction. The second and third term characterize the collisional depopulation and population, respectively, of the energy level in question with ω being the collision frequency and P_{ij} the probability for a transition $E_i \leftarrow E_j$. Finally, the last term describes the unimolecular reaction steps of the energized adduct with the specific rate constants $k_{r,i} = k_r(E_i)$ for the reaction pathway r. The energy, in general, is counted from the rovibrational ground state of HOOCl.

Equation 13 can be cast into matrix form,[40,44] and assuming steady-state conditions,[45] $dn_i/dt = 0$, one obtains

$$R_{form}\mathbf{F} = [\omega(\mathbf{I} - \mathbf{P}) + \sum_r \mathbf{K}_r]\mathbf{N}^s \equiv \mathbf{J}\mathbf{N}^s \tag{14}$$

where the vector/matrix symbols correspond to the symbols in eq 13, and **I** denotes the unit matrix. The steady-state population $\mathbf{N}^s$ now follows by inversion of the matrix **J** as

$$\mathbf{N}^s = R_{form}\mathbf{J}^{-1}\mathbf{F} \tag{15}$$

and the rate of the rth unimolecular step, D_r, is obtained by averaging the rate constants $k_{r,i}$ over this distribution:

$$D_r = \sum_i (\mathbf{K}_r\mathbf{N}^s)_i \tag{16}$$

The symbol $(\mathbf{X})_i$ formally stands for the ith diagonal element of a matrix **X**. Combination of eqs 15 and 16 leads to the relative branching fractions

$$\frac{D_r}{R_{form}} = \sum_i (\mathbf{K}_r\mathbf{J}^{-1}\mathbf{F})_i \tag{17}$$

and the yield of the stabilized intermediate is obtained from mass conservation, $R_{form} = D_{-1} + D_{1a'} + D_{1b'} + S$, as being

$$\frac{S}{R_{form}} = 1 - \sum_r \frac{D_r}{R_{form}} \tag{18}$$

In this way, all branching ratios of interest can be calculated.

The measurable bimolecular rate constant at a given temperature and pressure, $k_1(T,P)$, can be related to the corresponding capture or high-pressure limiting value, $k_1^\infty(T)$, by the relation

$$k_1(T,P) = k_1^\infty(T)\left[1 - \frac{D_{-1}(T,P)}{R_{form}(T)}\right] \tag{19}$$

Here, k_1 is expressed as the product of the pressure independent capture rate constant and a yield factor, which can be calculated from eq 17 and which characterizes the fraction of the intermediates that does not redissociate (see, e.g., ref 35). One

TABLE 4: Rotational Constants and Frequencies Used in the Modeling Calculations

species	*A*, *B*, *C* (cm^{-1})	ν_i (cm^{-1})
OH	18.91[a]	3738[a]
OD	10.02[b]	2721[b]
ClO	0.623[a]	854[a]
HO_2	20.82, 1.154, 1.097[c]	3459, 1370, 1161[c]
DO_2	11.40, 1.087, 0.993[c]	2548, 1173, 1009[c]
HOOCl	1.606, 0.201, 0.182[d]	3589, 1372, 851, 610, 407, 353[d]
DOOCl	1.454, 0.193, 0.175[d]	2615, 1013, 850, 609, 361, 292[d]
$HCl-O_2$[e]	1.213, 0.139, 0.125[d]	3154, 1494, 972, 443, 189[d]
$DCl-O_2$[e]	1.117, 0.138, 0.124[d]	2299, 1129, 928, 396, 185[d]

[a] Reference 54. [b] Reference 55. [c] Calculated ab initio at the UMP2/6-311+G(d,p) level with Gaussian 94,[56] frequencies scaled by a factor of 0.943.[57] The values for HO_2 agree very well with experimental data given in ref 58. [d] Reference 19. [e] Transition state of reaction 1b′.

should note that the temperature dependence of k_1 is a combined effect of the temperature dependence of both k_1^∞ and the yield factor, whereas the pressure dependence is only governed by the latter. The quantity R_{form} does not need to be specified, because it only implicitly appears within the ratios D_r/R_{form}. For ClO + OH, it would follow that $R_{form} = k_1^\infty(T)$[ClO][OH], and because this represents a capture rate, it is not pressure dependent.

The methods applied for the calculation of the different quantities in eqs 13−17 are briefly described next. The nascent population of HOOCl, $f(E)$, is approximated by a shifted thermal distribution[40−42]

$$f(E) = \frac{W_{HOOCl}(E - E_{0(-1)}) \exp\left[\frac{-(E - E_{0(-1)})}{k_B T}\right]}{\int_0^\infty W_{HOOCl}(\varepsilon) \exp\left(\frac{-\varepsilon}{k_B T}\right) d\varepsilon} \quad (20)$$

where $E_{0(-1)}$ represents the threshold energy for reaction −1 and W_{HOOCl} denotes the sum of states of HOOCl; k_B is Boltzmann's constant. The specific unimolecular rate constants are calculated by statistical rate theory as[40−42,46]

$$k_r(E) = \frac{W_r(E - E_{0(r)})}{h\rho_{HOOCl}(E)} \quad (21)$$

with the density of states of the intermediate ρ_{HOOCl} and Planck's constant h. For the number of open reaction channels W_r, one has to distinguish between two different cases. Reactions −1 and 1a′ are simple bond fissions and W_r is calculated by the statistical adiabatic channel model (SACM) in its simplified version.[47−49] Reaction 1b′, on the other hand, proceeds via a well-defined transition-state configuration,[19,36] and accordingly, $W_{1b'}$ is identified with its sum of states (RRKM model).[46]

All densities and sums of states are determined by direct counting procedures[49−51] for a total angular momentum quantum number $J = 15$. This value corresponds to an average, which can be estimated from the angular momenta of the reactants and the orbital angular momentum associated with the capture process.[52,53] It turns out that the influence of J on the branching ratios is very weak within the range accessible at temperatures between 200 and 300 K ($5 \le J \le 25$). The molecular geometries and frequencies employed in our calculations are compiled in Table 4.

For the transition probabilities P_{ij}, a stepladder model obeying detailed balancing is used.[40−43] For the step size, we assume $\Delta E_{SL} = 100$ cm^{-1}, which corresponds to an average energy

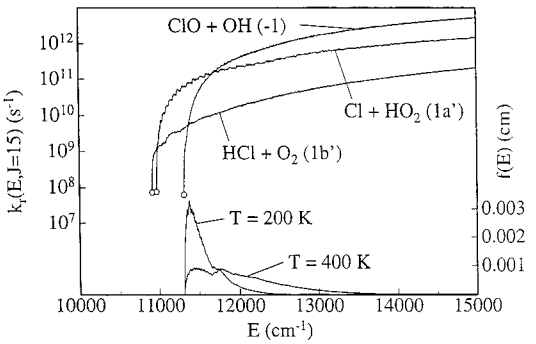

Figure 4. Specific rate constants for the different decomposition pathways and nascent molecular distribution functions for HOOCl generated from OH + ClO at two different temperatures. The open circles mark the threshold rate constants $k_r(E_{0(r)})$.

transferred per collision of about −20 cm^{-1}.[59] This is a reasonable value compared to other molecules of similar excitation energy and size.[60] Moreover, it turns out that the calculated branching ratios are again quite insensitive to this quantity (see below). The collision frequency of HOOCl in air, ω, is based on a Lennard-Jones collision number of 1×10^7 $Torr^{-1}$ s^{-1} at 300 K.[61] The inversion of the tridiagonal matrix **J** is achieved by standard procedures[62] with a grain size of 10 cm^{-1}.

The relative branching fraction (yield) for the channel leading to HCl + O_2 is expressed as

$$Y_{1b'} = \frac{D_{1b'}}{D_{1a'} + D_{1b'} + S} \quad (22)$$

It is accessible via eqs 17 and 18, where the rate of formation, R_{form}, cancels. One should note that D_{-1} is missing in the denominator, because it merely represents the reaction back to OH + ClO and, therefore, must not be included in the balance governing $Y_{1b'}$.

As already mentioned, the specific rate constants for the dissociation reactions −1 and 1a′ are calculated by the statistical adiabatic channel model. With the molecular data for the reactants and reaction products from Table 4 and the thermochemical data given above, there remains one parameter to be fixed, the so-called anisotropy ratio α/β.[47−49] In principle, this quantity could be adjusted to thermal high-pressure limiting rate constants for the corresponding association reactions. However, obviously the measured rate constants for OH + ClO and HO_2 + Cl do not represent high-pressure limits but are decreased by falloff effects (see below). Hence, we generally employ a value of $\alpha/\beta = 0.5$ in our calculations. It was shown[63,64] that in many cases, specific as well as the corresponding thermally averaged dissociation and recombination rate constants can be predicted reasonably well by using this "standard" value. The specific rate constants obtained in this way for the reactions −1 and 1a′ are shown in Figure 4.

Reaction 1b′, which proceeds through a tight transition state, is described by RRKM theory. The molecular parameters used are compiled in Table 4. The $TS_{(1b')}$ molecular parameters in Table 4 are from the ab initio calculations reported in ref 19. As already discussed in ref 19, the calculation of a reliable barrier height for the four-center transition state involved is not without problems. Therefore, we treat $E_{0(1b')}$ as an adjustable parameter, which is fitted so as to reproduce the observed relative yield $Y_{1b'} = 0.07 \pm 0.03$ at $T = 300$ K. A value of 31.1 ± 0.6 kcal mol^{-1} is obtained. This lies ∼1.2 kcal mol^{-1} below the thermochemical limit at 0 K for OH + ClO and essentially

TABLE 5: Relative Branching Fractions for HOOCl (DOOCl) Formed from OH (OD) + ClO, $P = 100$ Torr, $\Delta E_{SL} = 100$ cm^{-1} (exp: Experimental Values)

	HOOCl					DOOCl	
T (K)	D_{-1}/R_{form}	$D_{1a'}/R_{form}$	$D_{1b'}/R_{form}$	$Y_{1b'}$	$Y_{1b'}$(exp)	$Y_{1b'}$	$Y_{1b'}$(exp)[a]
200	0.3010	0.6506	0.0484	0.0693		0.0588	0.06 ± 0.02[b]
250	0.3733	0.5831	0.0436	0.0695	0.07 ± 0.03	0.0599	
300	0.4362	0.5241	0.0396	0.0703		0.0613	0.05 ± 0.02
400	0.5341	0.4319	0.0340	0.0730		0.0647	

[a] Reference 1. [b] $T = 210$ K.

agrees with the results from ref 19. The corresponding specific rate constants are also shown in Figure 4.

The calculated branching fractions from eq 17 and the relative yields $Y_{1b'}$ from eq 22 are compiled in Table 5. It is evident that the temperature dependence of $Y_{1b'}$ is very weak, which is in agreement with the experimental findings. The reason becomes clear by inspection of Figure 4. The curves of the specific rate constants for the two product channels, HCl + O_2 and Cl + HO_2, do not cross and are nearly parallel in the energy range, where the main part of the HOOCl population is located. Consequently, a shift of this population to higher energies by increasing the temperature will hardly change the branching ratio. Whether the ratio is slightly decreasing (as might be suggested by the experiments with the deuterated species,[1] cf. also Table 5) or increasing (as suggested by the present calculations) cannot be decided unambiguously. Here, much more detailed information on the properties of $TS_{(1b')}$ and on the adiabatic channel pattern for reaction 1a′ is required, where especially the latter is beyond the capabilities of current quantum chemical calculations.

Table 5 also shows that the influence of deuteration turns out to be very weak. The calculated yields $Y_{1b'}$ for OD + ClO are, on an absolute scale, only ∼1% lower than those for OH + ClO. This is again in agreement with the experimental findings.

By averaging the specific rate constants over the molecular distributions, a lifetime of ∼5 ps can be estimated for the vibrationally excited HOOCl* generated from ClO + OH. Therefore, collisional stabilization is negligible under atmospheric conditions, and the branching ratios are virtually independent of pressure. For instance, at $P = 100$ Torr, the relative fraction of stabilized HOOCl lies between 1×10^{-6} and 1×10^{-7} in the temperature range 200−400 K, and at $T =$ 300 K, the HCl + O_2 yield increases from 0.070 30 at 1 Torr to 0.070 35 at 760 Torr. This general picture is also not influenced by a change of the energy-transfer parameter of the stepladder model.

Equation 19 and the values for D_{-1}/R_{form} from Table 5 reveal that the overall rate constant for OH + ClO under atmospheric conditions is not in its high-pressure limit, since ∼30 to ∼45% redissociation occurs, depending on the temperature. Consequently, a comparison of the predicted and observed overall rate constants is useful in order to evaluate the quality of our model and to derive additional information on the reaction mechanism. Furthermore, it can be shown from eq 19 that the pressure dependence of the rate constant k_1 is governed solely by the relative branching fraction D_{-1}/R_{form}. The latter, however, proves nearly independent of pressure. For example, at $T =$ 300 K, it varies from 0.4359 to 0.4363 upon increasing the pressure from 1 to 760 Torr (see the discussions above). Thus, the pressure dependence of k_1 is negligible in this range.

Whereas the yield factor in eq 19 follows from the master equation, the high-pressure limiting rate constant, $k_1^{\infty}(T)$, is calculated directly from the canonical version of the SACM.[48,63] For reaction 1, OH + ClO → HOOCl*, it can be written as[63]

$$k_1^{\infty}(T) = k_1^{PST}(T) f_1^{rigid}(T) \tag{23}$$

Here, the first factor,

$$k_1^{PST}(T) = \frac{k_B T}{h}\left(\frac{h^2}{2\pi\mu k_B T}\right)^{3/2} \frac{Q_{el}(HOOCl)}{Q_{el}(OH)Q_{el}(ClO)} Q_{cent} \tag{24}$$

represents the rate constant in the loose or phase-space limit, i.e., in a purely isotropic potential, and a rigidity factor, $f_1^{rigid} \leq 1$,[63,65,66] globally accounts for the anisotropy. In eq 24, μ denotes the reduced mass of OH and ClO and Q_{el} the corresponding electronic partition functions. For the discussion of the temperature dependence of k_1^{∞}, one can essentially concentrate on k_1^{PST}, since the rigidity factors are often only slightly temperature dependent.[65,66] Thus, provided the electronic partition functions are known, the main task remaining is the determination of the centrifugal partition function Q_{cent}. It can be calculated from the maxima, $E_{0(1)}(J)$, of the effective potential

$$V_{eff}(q) = V(q) + B_{cent}(q)J(J+1) \tag{25}$$

as follows:

$$Q_{cent}(T) = \sum_{J=0}^{\infty}(2J+1)\exp\left(-\frac{E_{0(1)}(J) - E_{0(1)}(J=0)}{k_B T}\right) \tag{26}$$

where q is the interfragment distance between OH and ClO. In the original version of the simplified SACM,[48,49] a Morse potential was adopted for $V(q)$ and approximate expressions for the effective rotational constant, B_{cent}, were employed. In our calculations, we used the quasitriatomic model for the latter,[48] and the rigidity factors as given in ref 63 (formally multiplied by a factor Q^*_{cent}/Q_{cent}, because eq 24 contains Q_{cent} instead of Q^*_{cent} used in ref 63). All electronic partition functions were set identical to the corresponding ground-state degeneracy[55] with the exception of OH/OD, for which the partition function was calculated with a spin−orbit splitting of 139.7 cm^{-1}.[55]

The results are shown in Figure 5. One can realize that the predicted rate constants based on a Morse potential and a value of $\alpha/\beta = 0.5$, k_1^{MO}, are likely to be somewhat too small, and their temperature dependence is probably too weak. The latter is a known deficiency of this simple approximation, and the situation can be improved by using a more adequate interfragment potential.[68]

Because both OH and ClO have comparably large dipole moments ($\mu_{OH} = 1.66$ D, $\mu_{ClO} = 1.24$ D),[54] the corresponding long-range electrostatic interaction is a better description of the potential range that governs the capture process. From the isotropic part of the dipole−dipole interaction, it follows $V(q) = -2\mu_{OH}\mu_{ClO}/q^3$ and the centrifugal rotational constant becomes

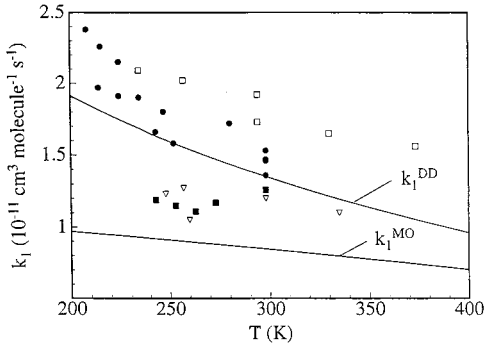

Figure 5. Calculated and reported experimental rate constants for the reaction OH + ClO. Experiments: ■, Burrows et al.;[21] □, Hills and Howard;[22] ●, Lipson et al.;[1] ▽, Ravishankara et al.[67] The calculated values are based on a Morse (k_1^{MO}) and a dipole−dipole (k_1^{DD}) potential for k_1^{∞}, respectively (see text).

$B_{cent}(q) = \hbar^2/(2\mu q^2)$.[69,70] For such types of effective potentials, the evaluation of Q_{cent} is straightforward, because the maxima, $E_{0(1)}(J)$, can be calculated analytically.[69] It turns out that in the temperature range from 200 to 400 K, the average (Boltzmann weighted) J in Q_{cent} varies from 49 to 55. The corresponding maxima of the effective potential, $E_{0(1)}(J = 49)$ and $E_{0(1)}(J = 55)$, are located at interfragment distances of 9.6×10^{-10} and 7.7×10^{-10} m, respectively. That is, the main part of Q_{cent} is indeed sampled over a range, where the dipole−dipole interaction is likely to provide the dominating contribution to the potential energy and where valence forces to a first approximation can be neglected. The rate constants, k_1^{DD}, obtained in this way are also shown in Figure 5. Here, a rigidity factor $f_1^{rigid} \approx 0.354$ was used,[71] which is independent of temperature for a pure dipole−dipole interaction.[71] The agreement with the experimental data is reasonable, and we note again that the only adjustable parameter is $E_{0(1b')}$. Because the dipole−dipole potential is probably more adequate than the Morse potential, our calculations favor the experimental rate constants with the stronger temperature dependence.

The influence of deuteration on the recombination rate is potentially underestimated by the calculations. In our earlier work[1] an isotope effect of $k_1(OH + ClO)/k_1(OD + ClO) \approx 1.4$ was determined experimentally in the temperature range 200−300 K. From our model, based on the dipole−dipole potential, a value of ≈ 1.03 is obtained. However, it is important to note that the uncertainty in this determination is large, since it involves independent measurements of OH and OD decays; hence, considering the experimental error, a value of 1.03 is not excluded by the measurements. Considering furthermore the uncertainties in the calculations, the predicted isotope effect and the measured isotope effect for k_1 are in reasonable agreement. Nonetheless, it is interesting to raise the question of whether the rather small isotope dependence of the branching ratio $Y_{1b'}$ given above can be correctly predicted (cf. Table 5). The situation is most conveniently analyzed in terms of eq 19. Here, one has to distinguish between the influence of the isotopic substitution on the capture rate constant, k_1^{∞}, and on the yield factor, $(1 - D_{-1}/R_{form})$. From our model, the respective ratios due to isotopic substitution are ≈1.02 and ≈1.01. Because the influence on k_1^{∞} is mainly governed by the mass difference of the two isotopomers, the effect is small and probably reproduced in the correct order of magnitude by the SACM approach. The main influence on the yield factor, on the other hand, is caused by the shift of the threshold energies relative to each other due to the different zero-point energies of the isotopomers. Inspection of Figure 4 reveals that the location of the crossing point of the two curves $k_{-1}(E)$ and $k_{1a'}(E)$ sensitively governs the yield D_{-1}/R_{form} for HOOCl formed from OH + ClO and in this way affects the recombination rate constant k_1. Small uncertainties in the threshold energies would lead to slightly different energy dependencies of $k_r(E)$, as becomes obvious from eq 21. Because of the similar slopes of $k_{-1}(E)$ and $k_{1a'}(E)$ near the crossing point, the location of the latter could be considerably shifted even by these small uncertainties, and therefore, the rate constant k_1 is strongly influenced. On the other hand, the branching between Cl + HO_2 and HCl + O_2 is much less sensitive to variations in $E_{0(r)}$, because at the relevant energies above $E_{0(-1)}$, the corresponding curves, $k_{1a'}(E)$ and $k_{1b'}(E)$, are nearly parallel. Therefore, small uncertainties in the differences of the zero-point energies for the two isotopomers may have a stronger influence on the rate constant k_1 than on the branching fraction $Y_{1b'}$. For instance, if the threshold $E_{0(-1)}$ is lowered by 270 cm^{-1} from 11 310 to 11 040 cm^{-1} (cf. Figure 4), the rate constant for OH + ClO decreases by a factor of 1.38, which is on the order of the observed isotope effect. The HCl yield thereby increases from 0.0703 to 0.0928. The HCl yield, though not drastically changed, is increased here because only $E_{0(-1)}$ was lowered. This simple variation is shown here only to demonstrate the sensitivity of the different quantities with respect to the energetic parameters and does not correspond to our model for OD + ClO.

In principle, the proposed model should also be capable of characterizing the kinetic behavior of the complementary reaction, HO_2 + Cl. For this reaction, an overall rate constant of $\sim 4.2 \times 10^{-11}$ cm^3 $molecule^{-1}$ s^{-1} is recommended.[38] It is nearly independent of temperature and pressure in the range 250−400 K and 1−760 Torr.[38] Relative branching fractions of 0.21 ± 0.016[72] and 0.18 ± 0.06[73] for the channel leading to OH + ClO have been determined experimentally at temperatures near 300 K. Our SACM approach based on a Morse potential with $\alpha/\beta = 0.5$ leads to a high-pressure rate constant of 2.3×10^{-11} cm^3 $molecule^{-1}$ s^{-1}. A yield factor of 0.3 (70% redissociation) finally results in a measurable rate constant of 6.9×10^{-12} cm^3 $molecule^{-1}$ s^{-1}, which is too low by a factor of 6 as compared to the experimental value. One reason might be that the predicted high-pressure recombination rate constant is too small. However, even in the phase-space limit, the calculated observable rate constant stays below the experimental value. Moreover, the relative branching fraction for the OH + ClO channel is overestimated. A value of 0.70 is obtained with $\alpha/\beta = 0.5$, and in the phase-space limit, it is merely decreased to 0.55, which is still too high. We were only able to bring the calculated and experimental rate constants and branching ratios closer to each other, if a parallel direct abstraction channel, HO_2 + Cl → HCl + O_2, is assumed so as to reproduce the measured overall rate constant. Then, with the above values for the branching ratios, a yield of 0.12 for the OH + ClO channel would be obtained ($0.7 \times 6.9 \times 10^{-12}/4.2 \times 10^{-11}$). To reproduce the experimental branching fractions near 0.20,[72,73] the high-pressure rate constant for HO_2 + Cl → HOOCl would have to be increased to $\sim 4 \times 10^{-11}$ cm^3 $molecule^{-1}$ s^{-1}. This is a factor of 2 higher than the value obtained above with the Morse function; however, as was already demonstrated for OH + ClO, deviations on this order of magnitude can well arise from the approximate nature of the intermolecular potential. Moreover, in the case of HO_2 + Cl, the long-range electrostatic interactions are too weak to provide a reasonable basis for the description of the centrifugal maxima, and detailed channel potentials for intermediate distances are required. Present quantum chemical methods are not accurate enough to make

the latter accessible; therefore, these considerations remain essentially qualitative in character for the time being. Nevertheless, our calculations indicate that a direct reaction path, $HO_2 + Cl \rightarrow HCl + O_2$, cannot be ruled out in addition to the association−elimination route.

Conclusions

The results presented here have established the kinetic significance of the minor channel for the OH + ClO reaction. The branching ratio involving the production of HCl was determined to be 7% under stratospheric conditions. Statistical rate theory calculations have demonstrated that theoretical predictions are in good agreement with the experimental results. Numerous atmospheric modeling studies have proposed that a branching ratio close to 7% would resolve discrepancies between measured and calculated chlorine partitioning in the upper stratosphere and help to resolve some of the discrepancies between measured and calculated O_3 concentrations, especially near 40 km. This work should help to improve modeling of O_3 levels in the upper stratosphere by placing more stringent constraints on the partitioning of stratospheric chlorine.

Acknowledgment. This research was funded by a grant from NASA Upper Atmosphere Research Program. M.O. would like to thank Prof. K. Scherzer for continuous support. J.B.L. acknowledges partial support from the NSF Training Grant in Chemistry of the Environment.

References and Notes

(1) Lipson, J. B.; Elrod, M. J.; Beiderhase, T. W.; Molina, L. T.; Molina, M. J. *J. Chem. Soc., Faraday Trans.* **1997**, *93*, 2665.
(2) Brasseur, G.; De Rudder, A.; Tricot, C. *J. Atmos. Chem.* **1985**, *3*, 261.
(3) McElroy, M. B.; Salawitch, R. J. *Science* **1989**, *243*, 763.
(4) Natarajan, M.; Callis, L. B. *J. Geophys. Res.* **1991**, *96*, 9361.
(5) Stachnik, R. A.; Hardy, J. C.; Tarsala, J. A.; Waters, J. W. *Geophys. Res. Lett.* **1992**, *19*, 1931.
(6) Eluszkiewicz, J.; Allen, M. *J. Geophys. Res.* **1993**, *98*, 1069.
(7) Chandra, S.; Jackman, C. H.; Douglass, A. R.; Fleming, E. L.; Considine, D. B. *Geophys. Res. Lett.* **1993**, *20*, 351.
(8) Toumi, R.; Bekki, S. *Geophys. Res. Lett.* **1993**, *20*, 2447.
(9) Siskind, D. E.; Connor, B. J.; Eckman, R. S.; Remsberg, E. E.; Tsou, J. J.; Parrish, A. *J. Geophys. Res.* **1995**, *100*, 11191.
(10) Eckman, R. S.; Grose, W. L.; Turner, R. E.; Blackshear, W. T.; Russell, J. M., III; Froidevaux, L.; Waters, J. W.; Kumer, J. B.; Roche, A. E. *J. Geophys. Res.* **1995**, *100*, 13951.
(11) Dessler, A. E.; Kawa, S. R.; Considine, D. B.; Waters, J. W.; Froidevaux, L.; Kumer, J. B. *Geophys. Res. Lett.* **1996**, *23*, 339.
(12) Osterman, G. B.; Salawitch, R. J.; Sen, B.; Toon, G. C.; Stachnik, R. A.; Pickett, H. M.; Margitan, J. J.; Blavier, J.-F.; Peterson, D. B. *Geophys. Res. Lett.* **1997**, *24*, 1107.
(13) Khosravi, R.; Brasseur, G. P.; Smith, A. K.; Rusch, D. W.; Waters, J. W.; Russell, J. M., III. *J. Geophys. Res.* **1998**, *103*, 16203.
(14) Allen, M.; Delitsky, M. L. *J. Geophys. Res.* **1991**, *96*, 2913.
(15) Chance, K.; Traub, W. A.; Johnson, D. G.; Jucks, K. W.; Ciarpallini, P.; Stachnik, R. A.; Salawitch, R. J.; Michelsen, H. A. *J. Geophys. Res.* **1996**, *101*, 9031.
(16) Michelsen, H. A.; Salawitch, R. J.; Gunson, M. R.; Aellig, C.; Kämpfer, N.; Abbas, M. M.; Abrams, M. C.; Brown, T. L.; Chang, A. Y.; Goldman, A.; Irion, F. W.; Newchurch, M. J.; Rinsland, C. P.; Stiller, G. P.; Zander, R. *Geophys. Res. Lett.* **1996**, *23*, 2361.
(17) Chang, A. Y.; Salawitch, R. J.; Michelsen, H. A.; Gunson, M. R.; Abrams, M. C.; Zander, R.; Rinsland, C. P.; Elkins, J. W.; Dutton, G. S.; Volk, C. M.; Webster, C. R.; May, R. D.; Fahey, D. W.; Gao, R.-S.; Loewenstein, M.; Podolske, J. R.; Stimpfle, R. M.; Kohn, D. W.; Proffitt, M. H.; Margitan, J. J.; Chan, K. R.; Abbas, M. M.; Goldman, A.; Irion, F. W.; Manney, G. L.; Newchurch, M. J.; Stiller, G. P. *Geophys. Res. Lett.* **1996**, *23*, 2393.
(18) Jucks, K. W.; Johnson, D. G.; Chance, K. V.; Traub, W. A.; Salawitch, R. J.; Stachnik, R. A. *J. Geophys. Res.* **1996**, *101*, 28785.
(19) Dubey, M. K.; McGrath, M. P.; Smith, G. P.; Rowland, F. S. *J. Phys. Chem. A* **1998**, *102*, 3127.
(20) Leu, M. T.; Lin, C. L. *Geophys. Res. Lett.* **1979**, *6*, 425.
(21) Burrows, J. P.; Wallington, T. J.; Wayne, R. P. *J. Chem. Soc., Faraday Trans. 2* **1984**, *80*, 957.
(22) Hills, A. J.; Howard, C. J. *J. Chem. Phys.* **1984**, *81*, 4458.
(23) Poulet, G.; Laverdet, G.; Le Bras, G. *J. Phys. Chem.* **1986**, *90*, 159.
(24) Sandor, B. J.; Clancy, R. T.; Rusch, D. W.; Randall, C. E.; Eckman, R. S.; Siskind, D. S.; Muhleman, D. O. *J. Geophys. Res.* **1997**, *102*, 9013.
(25) Summers, M. E.; Conway, R. R.; Siskind, D. E.; Stevens, M. H.; Offermann, D.; Riese, M.; Preusse, P.; Strobel, D. F.; Russell, J. M., III. *Science* **1997**, *277*, 1967.
(26) Seeley, J. V.; Jayne, J. T.; Molina, M. J. *Int. J. Chem. Kinet.* **1993**, *25*, 571.
(27) Seeley, J. V. Experimental Studies of Gas Phase Radical Reactions Using the Turbulent Flow Tube Technique. Ph.D. Thesis, Massachusetts Institute of Technology, 1994.
(28) Seeley, J. V.; Jayne, J. T.; Molina, M. J. *J. Phys. Chem.* **1996**, *100*, 4019.
(29) DeMore, W. B.; Sander, S. P.; Howard, C. J.; Ravishankara, A. R.; Golden, D. M.; Kolb, C. E.; Hampson, R. F.; Kurylo, M. J.; Molina, M. J. *Chemical Kinetics and Photochemical Data for Use in Stratospheric Modeling*; JPL Publication 97-4; Jet Propulsion Laboratory: Pasadena, CA, 1997.
(30) Seeley, J. V.; Meads, R. F.; Elrod, M. J.; Molina, M. J. *J. Phys. Chem.* **1996**, *100*, 4026.
(31) Mallard, W. G.; Westley, F.; Herron, J. T.; Hampson, R. F. *NIST Chemical Kinetics Database Version 6.0*; NIST Standard Reference Data; NIST: Gaithersberg, MD, 1994.
(32) Elrod, M. J.; Meads, R. F.; Lipson, J. B.; Seeley, J. V.; Molina, M. J. *J. Phys. Chem.* **1996**, *100*, 5808.
(33) Huey, L. G.; Hanson, D. R.; Howard, C. J. *J. Phys. Chem.* **1995**, *99*, 5001.
(34) Mozurkewich, M.; Benson, S. W. *J. Phys. Chem.* **1984**, *88*, 6429.
(35) Troe, J. *J. Chem. Soc., Faraday Trans.* **1994**, *90*, 2303.
(36) Weissman, M.; Shum, L. G. S.; Heneghan, S. P.; Benson, S. W. *J. Phys. Chem.* **1981**, *85*, 2863.
(37) Lee, T. J.; Rendell, A. P. *J. Phys. Chem.* **1993**, *97*, 6999.
(38) Atkinson, R.; Baulch, D. L.; Cox, R. A.; Hampson, R. F., Jr.; Kerr, J. A.; Troe, J. *J. Phys. Chem. Ref. Data* **1992**, *21*, 1125.
(39) Howard, C. J. *J. Am. Chem. Soc.* **1980**, *102*, 6937. See also: Fisher, E. R.; Armentrout, P. B. *J. Phys. Chem.* **1990**, *94*, 4396.
(40) Robinson, P. J.; Holbrook, K. A. *Unimolecular Reactions*; Wiley: New York, 1972. Holbrook, K. A.; Pilling, M. J.; Robertson, S. H. *Unimolecular Reactions*, 2nd ed.; Wiley: Chichester, U.K., 1996.
(41) Forst, W. *Theory of Unimolecular Reactions*; Academic Press: New York, 1972.
(42) Gilbert, R. G.; Smith, S. C. *Theory of Unimolecular and Recombination Reactions*; Blackwell: Oxford, U.K., 1990.
(43) Rabinovitch, B. S.; Diesen, R. E. *J. Chem. Phys.* **1959**, *30*, 735. Rabinovitch, B. S.; Kubin, R. F.; Harrington, R. E. *J. Chem. Phys.* **1963**, *38*, 405.
(44) Hoare, M. *J. Chem. Phys.* **1963**, *38*, 1630.
(45) Schranz, H. W.; Nordholm, S. *Chem. Phys.* **1984**, *87*, 163.
(46) Marcus, R. A.; Rice, O. K. *J. Phys. Colloid Chem.* **1951**, *55*, 894. Marcus, R. A. *J. Chem. Phys.* **1952**, *20*, 359.
(47) Quack, M.; Troe, J. *Ber. Bunsen-Ges. Phys. Chem.* **1974**, *78*, 240.
(48) Troe, J. *J. Chem. Phys.* **1981**, *75*, 226.
(49) Troe, J. *J. Chem. Phys.* **1983**, *79*, 6017.
(50) Beyer, T.; Swinehart, D. F. *Comm. Assoz. Comput. Mach.* **1973**, *16*, 379. Astholz, D. C.; Troe, J.; Wieters, W. *J. Chem. Phys.* **1979**, *70*, 5107.
(51) Olzmann, M.; Troe, J. *Ber. Bunsen-Ges. Phys. Chem.* **1992**, *96*, 1327; **1994**, *98*, 1563.
(52) Pechukas, P.; Light, J. C. *J. Chem. Phys.* **1965**, *42*, 3281.
(53) Olzmann, M. *Ber. Bunsen-Ges. Phys. Chem.* **1997**, *101*, 533.
(54) Radzig, A. A.; Smirnov, B. M. *Reference Data on Atoms, Molecules, and Ions*; Springer Series in Chemical Physics 31; Springer-Verlag: Berlin, 1985.
(55) Herzberg, G. Molecular Spectra and Molecular Structure, Vol. I; *Spectra of Diatomic Molecules*; van Nostrand: Princeton, NJ, 1950.
(56) Frisch, M. J.; Trucks, G. W.; Schlegel, H. B.; Gill, P. M. W.; Johnson, B. G.; Robb, M. A.; Cheeseman, J. R.; Keith, T.; Petersson, G. A.; Montgomery, J. A.; Raghavachari, K.; Al-Laham, M. A.; Zakrzewski, V. G.; Ortiz, J. V.; Foresman, J. B.; Cioslowski, J.; Stefanov, B. B.; Nanayakkara, A.; Challacombe, M.; Peng, C. Y.; Ayala, P. Y.; Chen, W.; Wong, M. W.; Andres, J. L.; Replogle, E. S.; Gomperts, R.; Martin, R. L.; Fox, D. J.; Binkley, J. S.; Defrees, D. J.; Baker, J.; Stewart, J. P.; Head-Gordon, M.; Gonzalez, C.; Pople, J. A. *Gaussian 94*, Revision D.2; Gaussian Inc.: Pittsburgh, PA, 1995.
(57) Scott, A. P.; Radom, L. *J. Phys. Chem.* **1996**, *100*, 16502.
(58) Herzberg, G. Molecular Spectra and Molecular Structure, Vol. III; *Electronic Spectra and Electronic Structure of Polyatomic Molecules*; van Nostrand: Princeton, NJ, 1966.
(59) Snider, N. *J. Phys. Chem.* **1985**, *89*, 1257.

(60) Dove, J. E.; Hippler, H.; Troe, J. *J. Chem. Phys.* **1985**, *82*, 1907. Hippler, H. *Ber. Bunsen-Ges. Phys. Chem.* **1985**, *89*, 303. Heymann, M.; Hippler, H.; Nahr, D.; Plach, H. J.; Troe, J. *J. Phys. Chem.* **1988**, *92*, 5507. Cobos, C. J.; Troe, J. *Z. Phys. Chem. Neue Folge* **1992**, *176*, 161.

(61) Reid, R. C.; Prausnitz, J. M.; Poling, B. E. *The Properties of Gases and Liquids*; McGraw-Hill: New York, 1987.

(62) Press: W. H.; Flannery, B. P.; Teukolsky, S. A.; Vetterling, W. T. *Numerical Recipes*; Cambridge University Press: Cambridge, U.K., 1989.

(63) Cobos, C. J.; Troe, J. *J. Chem. Phys.* **1985**, *83*, 1010.

(64) Brouwer, L.; Cobos, C. J.; Troe, J.; Dübal, H.-R.; Crim, F. F. *J. Chem. Phys.* **1987**, *86*, 6171.

(65) Troe, J. *Z. Phys. Chem. Neue Folge* **1989**, *161*, 209.

(66) Troe, J. *Ber. Bunsen-Ges. Phys. Chem.* **1997**, *101*, 438.

(67) Ravishankara, A. R.; Eisele, F. L.; Wine, P. H. *J. Chem. Phys.* **1983**, *78*, 1140.

(68) Troe, J. *J. Phys. Chem.* **1986**, *90*, 3485; *Ber. Bunsen-Ges. Phys. Chem.* **1988**, *92*, 242.

(69) Levine, R. D.; Bernstein, R. B. *Molecular Reaction Dynamics and Chemical Reactivity*; Oxford University Press: Oxford, U.K., 1987.

(70) Troe, J. *Chem. Phys. Lett.* **1985**, *122*, 425.

(71) Maergoiz, A. I.; Nikitin, E. E.; Troe, J.; Ushakov, V. G. *J. Chem. Phys.* **1996**, *105*, 6277.

(72) Lee, Y.-P.; Howard, C. J. *J. Chem. Phys.* **1982**, *77*, 756.

(73) Cattell, F. C.; Cox, R. A. *J. Chem. Soc., Faraday Trans. 2* **1986**, *82*, 1413.